Modelling and control of a brake system for an extended range electric vehicle equipped with axle motors

Kerem Bayar*, Ricardo Biasini, Simona Onori and Giorgio Rizzoni

Centre for Automotive Research,
The Ohio State University,
930 Kinnear Rd., Columbus, OH 43212, USA
E-mail: bayar.2@osu.edu
E-mail: riccardo.biasini@gmail.com
E-mail: onori.1@osu.edu
E-mail: rizzoni.1@osu.edu
*Corresponding author

Abstract: This work focuses on modelling of an electro-hydraulic brake system for an extended range electric vehicle equipped with axle motors, and proposing an optimal braking strategy which utilises a two-layer split of braking action such that the desired braking force is first distributed to the front and rear axles in order to track the ideal brake force distribution factor and, then, to the electro-hydraulic friction brakes and electric motors in order to maximise energy recuperation. With simulation results, it is shown that the proposed regenerative braking strategy achieves the dual objective of ensuring a good dynamic performance and optimal energy recovery.

Keywords: HEV; hybrid electric vehicle; E-REV; extended-range electric vehicle; EV; electric vehicle; regenerative braking; motor braking; friction braking; EHB; electro-hydraulic braking; ideal brake force distribution; deceleration; energy optimisation; vehicle simulator.

Reference to this paper should be made as follows: Bayar, K., Biasini, R., Onori, S. and Rizzoni, G. (2012) 'Modelling and control of a brake system for an extended range electric vehicle equipped with axle motors', *Int. J. Vehicle Design*, Vol. 58, Nos. 2/3/4, pp.399–426.

Biographical notes: Kerem Bayar received the BS and MS degrees in Mechanical Engineering from Middle East Technical University, Ankara, Turkey, in 2004 and 2006, respectively. After an internship at the Automotive Engineering Institute of Technische Universitat Darmstadt, Germany, he started working as a PhD student and research assistant at Centre for Automotive Research, The Ohio State University, USA, in 2007. His area of interest is HEV and Vehicle Dynamics Control.

Riccardo Biasini got BS and MS degrees from Aerospace Engineering and Automotive Engineering, in 2008 and 2010, respectively, from University of Pisa, Italy. After internships at Fermi National Laboratory Accelerator, Dallara Automobili, and Centre for Automotive Research, he started working as powertrain modelling engineer at Tesla Motors, USA. His main area of interest is powertrain modelling for EVs.

Simona Onori is a Research Scientist at the Ohio State University Center for Automotive Research (CAR). She received her Laurea degree Summa Cum Laude in Computer Science Engineering from University of Rome 'Tor Vergata', MS in Electrical Engineering from University of New Mexico, and PhD in Automation Engineering from University of Rome 'Tor Vergata' in 2003, 2004 and 2007, respectively. She is an Associate Editor for the ASME Dynamics Systems and Control Conference and American Control Conference. Her research focuses on energy management control and optimisation for HEV and PHEV, fault diagnosis and prognosis with application to automotive systems, cloud computing based optimisation, aging and characterisation of advanced batteries.

Giorgio Rizzoni, the Ford Motor Company Chair in Electromechanical Systems, is a Professor of Mechanical and Aerospace Engineering and of Electrical and Computer Engineering, and Director of the Center for Automotive Research (an interdisciplinary research center supporting 30 full-time staff and 70 graduate students) at the Ohio State University. His research interests include dynamics, control and diagnosis of automotive systems, with emphasis on hybrid and electric vehicles, and on energy conversion and storage systems. He received his BS, MS and PhD degrees in Electrical and Computer Engineering from the University of Michigan and is a Fellow of IEEE and SAE.

1 Introduction

Regenerative braking is the means of recovering vehicle's kinetic energy during braking, transferring it in a special storage system and converting it back into energy for propulsion. In automotive applications, regenerative braking can be categorised according to the type of system used to store the energy. These devices include batteries or ultracapacitors (Yeo and Kim, 2002; Lu et al., 2007; Wang et al., 2007; Wang and Zhuo, 2008; Ye et al., 2008), hydraulic or pneumatic accumulators (Kepner, 2002; Britto et al., 2005), flywheel and elastomeric storage systems (Clegg, 1996; Diego-Ayala et al., 2008). Even though the concept of regenerative braking can be applied with different approaches to conventional vehicles, it finds full application only with Hybrid Electric Vehicles (HEVs).

One of the most important features of HEVs, including Plug-in Hybrid Electric Vehicles (PHEVs) and full-Electric Vehicles (EVs), is in their capability to capture kinetic energy from braking and convert it electrically to be stored into the energy storage device and used for providing propulsive power or for the basic energy needs of supplementary electrical systems. This is achieved without any additional cost: the electric motor works as generator, which ultimately saves fuel and improves fuel economy and reduces exhaust emissions.

On the other hand, regenerative braking cannot be applied as a standalone braking system in HEVs, PHEVs or EVs; it needs to be accompanied by the conventional friction brake system. This is because the maximum braking torque which can be provided by the electric motor is a decreasing function of the speed (Figure 1, area 1). Moreover, at low speed (Figure 1, area 2), the regenerative braking is not allowed because the electric motor would suffer from the ripples of torque generated and the power recovered would be no greater than that used to control the inverter and compensate for

electro-mechanical losses. Additionally, assistance of conventional friction braking is required when the energy management control strategy of the HEV prevents using regenerative braking, for instance at high State of Charge (SOC) or high temperature of the battery (Miller, 2004).

Figure 1 Qualitative illustration of the maximum or minimum electric motor torque as a function of motor speed (see online version for colours)

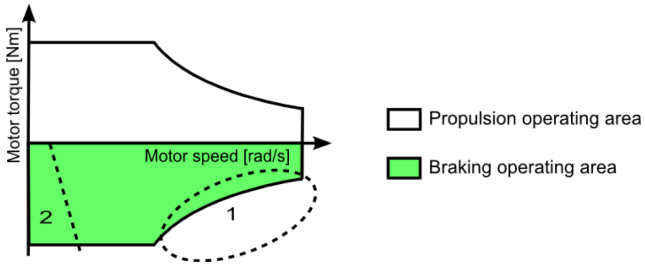

Friction brake system in HEVs may be hydraulically actuated by the effort of the driver who acts on the brake pedal, or Brake-By-Wire (BBW) type, that is controlled remotely. Electro-Hydraulic Braking (EHB) (Jonner et al., 1996; Nakamura et al., 2002) and Electro-Mechanical Braking (EMB) (Ueki et al., 2004) systems are two different types of BBW systems. The former is normally used on existing hybrid vehicles and it consists of a hydraulic circuit powered by a pump. The desired pressure inside the caliper is modulated by the valves which are electronically controlled (Tianjun and Changfu, 2009; Hongyan et al., 2009). A safety hydraulics circuit connects the brake pedal directly to the calipers in case of a malfunction of the by-wire part (D'alfio et al., 2006). The EMB system on the other hand commands the calipers electro-mechanically without the need of a hydraulic circuit (Xiang et al., 2008; Mamilla and Mallikarjun, 2009; Ahn et al., 2009). However this type of system does not have sufficient reliability yet to be installed on non-prototype vehicles.

During regenerative braking it is important to achieve the dual objective of ensuring a good dynamic performance of the vehicle and maximising the recuperated energy without sacrificing drivability. The main task of the regenerative braking strategy is to distribute the braking torque request between the braking devices. With a parallel regenerative braking strategy, electric motor braking and friction braking are applied simultaneously to provide the torque desired by the driver, as shown in Figure 2(a). Therefore depending on regenerative brake torque availability, the pedal feel changes which restricts the application of this strategy to micro or mild hybrids. The market vehicles equipped with parallel regenerative braking strategy can provide regenerative braking for usually less than around 0.08 g of deceleration request coming from the driver, and this restricts their fuel economy enhancement. One advantage of these systems though is that no additional hardware is needed at the top of conventional brake actuation (conventional master cylinder, brake pedal, ABS, ESP, etc.). Honda Accord HEV, Honda Civic HEV (Pre 06), Saturn Vue HEV (Pre 06), Saturn Aura HEV, Chevy Malibu HEV, and Hyundai Accent Hybrid are some examples of vehicles that apply parallel regenerative braking strategy.

Figure 2 A conceptual illustration of parallel and series regenerative braking strategies. Note that the tiny yellow band at the bottom of both figures represents regen for engine compression braking: (a) parallel regen strategy and (b) series regen strategy (see online version for colours)

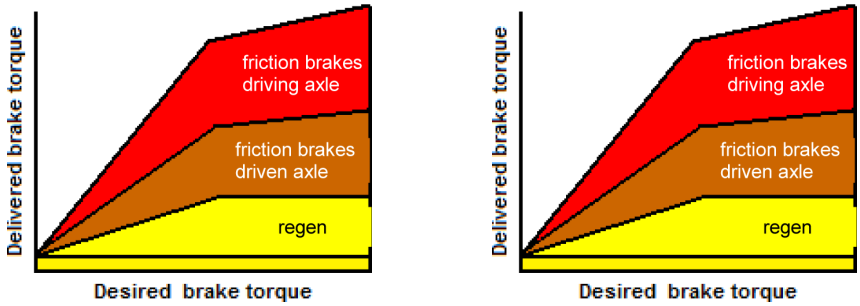

(a) (b)

Series regenerative braking strategy, on the other hand, utilises only electric motor braking up until the motor torque or vehicle stability limits are reached and, if the brake pedal is depressed more, the strategy commands friction brakes to satisfy the driver request, as shown in Figure 2(b). Therefore this strategy leads not only to the consistency of the pedal feel but also to the full utilisation of regenerative braking and this yields a better fuel economy enhancement in comparison to the parallel regen braking strategy. Some examples of Medium or Full hybrids (> 0.08 g regen deceleration capability) that apply series regenerative braking strategy are Ford Escape HEV, Toyota Prius, Toyota Camry HEV, Mercury Mariner HEV, Chevy Tahoe HEV, and GMC Yukon HEV. A BBW actuation system is needed though, if a series regenerative braking strategy is to be implemented.

Most of the HEVs in the market today that utilise series regen braking strategy have only one electric motor, generally connected to the front axle. The choice is usually such that front axle motor braking is applied for low deceleration events and conventional friction brakes are introduced for further braking demanded. This strategy has the following drawbacks:

- The vehicle may have an understeering (oversteering if the electric motor is connected to the rear axle) behaviour during braking which can cause an anticipated ABS or ESP action as also mentioned in the literature (Hancock and Assadian, 2006)
- The vehicle's kinetic energy could be dissipated by friction brakes before electric motor can reach the torque limit due to brake force distribution concerns (Hellgren and Jonasson, 2007).

In that context, this work focuses firstly on modelling of an Electro-Hydraulic Brake system (EHB) for a Hybrid SUV equipped with axle motors, secondly on proposing an optimal braking strategy that maximises the recuperated energy without deviating from the ideal brake force distribution factor. The EHB model is embedded to the vehicle simulator that has been developed at The Ohio State University, Centre for Automotive Research, developed within the EcoCAR Next Challenge project. The organisation of the paper is as follows: an analytical energy analysis on regenerative braking is performed

in Section 2 in order to have a better understanding of the domain of energy that can be recuperated with regenerative braking. In Section 3 the EcoCAR vehicle architecture is introduced. In Section 4, the EHB and the hybrid powertrain models are presented in the frame of the EcoDYN vehicle simulator. The optimal braking strategy is proposed which utilises a two-layer split of braking action such that the desired braking force is first distributed to the front and rear axles in order to track the ideal brake force distribution factor and, then, to the electro-hydraulic friction brakes and electric motors in order to maximise energy recuperation. In Section 5, simulations results for different braking manoeuvres and drive cycles are presented to evaluate the proposed braking strategy in terms of vehicle dynamics and a comparison to different braking strategies is performed, focusing on the energy recovered in the battery and the fuel consumption achieved. Finally, in Section 6, this study is concluded with some remarks and expected contributions to the art.

2 Energy analysis for regenerative braking

In this section, a preliminary energy analysis during braking of a vehicle is performed. This is done with the aim of reaching some quantitative results and drawing the domain of braking energy on which any regenerative braking strategy can act for different driving cycles.

During braking, there are several factors that contribute to the decreasing kinetic energy of the vehicle, as illustrated in Figure 3.

Figure 3 Resistances to motion (see online version for colours)

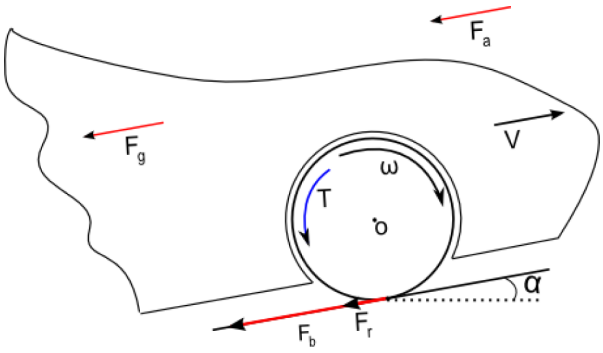

The equation of motion along the longitudinal direction of motion of the vehicle can be written as:

$$M\frac{\mathrm{d}V}{\mathrm{d}t} = -F_a - F_g - \sum_{i=1}^{4} F_{ri} - \sum_{i=1}^{4} F_{bi} \tag{1}$$

where M is the equivalent mass of the vehicle and V is the vehicle longitudinal velocity, F_a and F_g are the aerodynamic and grade resistances respectively, F_{ri} and F_{bi} are the rolling resistance and braking force for the ith wheel respectively. The resistances to motion can further be expressed as (Gillespie, 1992):

$$F_a = 0.5\rho C_d A_f V_r^2 \tag{2}$$

$$\sum_{i=4}^{4} F_{ri} = \mathrm{Mg}\cos(\alpha)(f_o + f_s V^{2.5}) \tag{3}$$

$$F_g = \mathrm{Mg\ Sin}(\alpha) \tag{4}$$

where ρ is the density of air, C_d is the aerodynamic coefficient, A_f is the frontal area, V_r is the relative velocity of the vehicle with respect to wind speed, f_o and f_s are rolling resistance coefficients and α is the road grade. The unit of velocity in equation (3) is kph. Assuming zero grade and no wind and substituting equations 2–4 into equation (1) and multiplying each term with velocity to obtain the power balance yields:

$$M\frac{\mathrm{d}V}{\mathrm{d}t}V = -0.5\rho C_d A_f V_r^3 - MgV\left(f_o + f_s V^{2.5}\right) - V\sum_{i=4}^{4} F_{bi}. \tag{5}$$

From the wheel dynamics, the braking force and braking torque can be related to each other as:

$$\frac{\mathrm{d}\omega_i}{\mathrm{d}t} = \frac{1}{I_w}(-T_{bi} + r_w F_{bi}) \tag{6}$$

where I_w is the rotational inertia and r_w is the rolling radius of the wheels respectively, and ω_i, T_{bi}, and F_{bi} represent the angular velocity, braking torque, and braking force for the ith wheel during braking respectively. Substituting the expression for F_{bi} in equation (6) into equation (5) yields:

$$V\frac{1}{r_w}\sum_{i=1}^{4} T_{bi} = -M\frac{\mathrm{d}V}{\mathrm{d}t}V - \frac{I_w}{r_w}V\sum_{i=1}^{4}\frac{\mathrm{d}\omega_i}{\mathrm{d}t} - 0.5\rho C_d A_f V_r^3 - MgV\left(f_o + f_s V^{2.5}\right). \tag{7}$$

Note that the longitudinal velocity (with the assumption of motion in only longitudinal direction) can be related to angular velocity of the wheel considering the slip equation as:

$$s_i = \frac{V - r_w\omega_i}{V} \tag{8}$$

Substituting $V=r_w\omega_i/(1 - s_i)$ into the term on the left hand side of equation (7) and $\mathrm{d}\omega_i/\mathrm{d}t=[(1-s_i)\mathrm{d}V/\mathrm{d}t - V\mathrm{d}s_i/\mathrm{d}t]/r_w$ into the second term on the right hand side yields:

$$\begin{aligned}\sum_{i=1}^{4}\frac{\omega_i T_{bi}}{1-s_i} = &-\left(M + \frac{4I_w}{r_w^2} - \frac{I_w}{r_w^2}\sum_{i=1}^{4} s_i\right)\frac{\mathrm{d}V}{\mathrm{d}t}V + \frac{I_w}{r_w^2}V^2\sum_{i=1}^{4}\frac{\mathrm{d}s_i}{\mathrm{d}t} \\ &- 0.5\rho C_d A_f V^3 - MgV(f_o + f_s V^{2.5}).\end{aligned} \tag{9}$$

To get the summation of four wheel slip values and their time rates of change, i.e., Σs_i and $\Sigma\dot{s}_i$, the knowledge of the drive cycle as a priori and the Pacejka tyre formula (Pacejka, 2003) for longitudinal force can be used. The normalised longitudinal force vs. longitudinal slip behaviour of the tyre with respect to the Pacejka model can be expressed by equation (10), and is shown in Figure 4.

$$\frac{F_x}{F_z} = \mu\sin(C_x\arctan(B_x s - E_x(B_x s - \arctan(B_x s)))) \tag{10}$$

where μ is the coefficient of adhesion, B_x, C_x and E_x are tyre parameters, and F_z is the normal load on the tyre.

Figure 4 Longitudinal force vs. slip characteristics (see online version for colours)

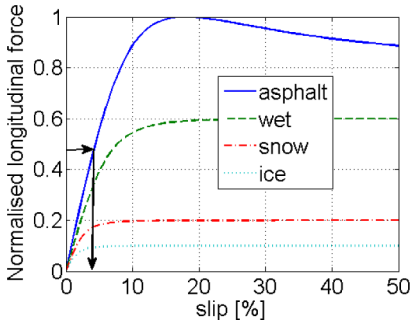

Note that taking the normal load as the weight of the vehicle, normalised longitudinal force can be treated also as the deceleration in units of g as an approximation. By means knowing the drive cycle (velocity and deceleration as a function of time) as a priori yields the knowledge of the total slip value (and its time rate of change) at each instant as a function of deceleration using the tyre characteristic in an inverse manner for each road surface, as shown by the arrows in Figure 4. Defining $\Sigma s_i = s_{total}$ and $\Sigma \dot{s}_i = \dot{s}_{total}$ and integrating both sides of equation (9) to find the energy yields:

$$\begin{aligned}\sum_{i=1}^{4}\int_{t_1}^{t_2}\omega_i T_{bi}\,\mathrm{d}t = &-\int_{t_1}^{t_2}\left(1-\frac{s_{total}(t)}{4}\right)\left[\left(M+\frac{I_w(4-s_{total}(t))}{r_w^2}\right)\frac{\mathrm{d}V}{\mathrm{d}t}V(t)-\frac{I_w}{r_w^2}V^2(t)\frac{\mathrm{d}s_{total}}{\mathrm{d}t}\right]\mathrm{d}t\\ &-\int_{t_1}^{t_2}\left(1-\frac{s_{total}(t)}{4}\right)0.5\rho C_d A_f V^3(t)\mathrm{d}t\\ &-\int_{t_1}^{t_2}\left(1-\frac{s_{total}(t)}{4}\right)\mathrm{M}gV(t)\left(f_o+f_s V^{2.5}(t)\right)\mathrm{d}t.\end{aligned} \tag{11}$$

Note that equation (11) gives the domain of potential braking energy that any regenerative braking strategy can act on during braking. It is the energy taken away by the brake system of the vehicle after other dissipative forces are subtracted from the drop in its total kinetic energy.

With the set of data given in Table 1, the change in kinetic energy of the vehicle (1st term on the right hand side of equation (11)) and the percentage of energy dissipated to aerodynamic (2nd term on the right hand side of equation (11)) and rolling (3rd term on the right hand side of equation (11)) resistances during braking and the remaining domain of energy that regenerative braking can act on for different drive cycles is tabulated in Table 2.[1]

This percentage of brake energy corresponds to 2.96 MJ, 0.59 MJ and 2.99 MJ for FUDS, FHDS and US06 respectively.[1] Therefore the urban driving cycle FUDS which contains deceleration schemes at low magnitudes and US06 that contains less frequent deceleration, occasionally at higher magnitudes, are the two drive cycles that have a higher potential for regenerative braking in comparison to the highway drive cycle FHDS which does not contain many deceleration schemes. With simulation results in Section 5,

it is analysed what portion of this energy is recuperated with the braking strategy proposed in this paper, and the results are discussed.

Table 1 Vehicle data used for the preliminary energy analysis

Equivalent mass	2215 kg
Aerodynamic coefficient	0.386
Vehicle frontal area	2.64 m^2
Density of air	1.2 kg/m^3
Tyre rolling radius	0.33 m
Wheel inertia	1.5 $kg.m^2$
f_o	0.01
f_s	4.93 10^{-8} $kph^{-2.5}$

Table 2 The change in kinetic energy and contribution of braking and dissipative resistances

	FUDS	*FHDS*	*US06*
ΔKE [MJ]	3.99	1.58	4.51
E_{aero}	7.6%	30.9	18.5%
E_{roll}	18.4%	31.6	15.2%
E_{brake}	74.0%	37.5	66.3%

3 EcoCAR vehicle

EcoCAR competition (EcoCAR,2008) is a program sponsored by General Motors and the United States Department of Energy with the aim of exploring means of achieving better fuel economy and lower emissions while maintaining safety, performance and utility through the use of advanced powertrain technologies. An Extended-Range Electric Vehicle (E-REV) was designed by the Ohio State team. This vehicle is equipped with a 1.8 L dedicated E85 engine, 82 kW front electric motor and a 103 kW rear electric motor, powered by A 21 kWh lithium ion battery pack (split into 5 parts for weight distribution and packaging issues). The vehicle architecture is shown in Figure 5. Details on design of this vehicle can be found in Bayar et al. (2010).

Figure 5 OSU EcoCAR vehicle architecture (see online version for colours)

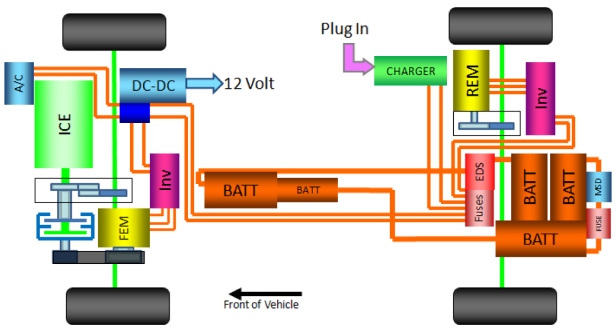

4 EcoDYN vehicle simulator

EcoDYN vehicle simulator is a dynamic model of this experimental HEV that is developed to facilitate the evaluation of control strategies in terms of vehicle dynamics, drivability, fuel economy and performance. The overall structure of the simulator is shown in Figure 6.

Different subsections of the simulator are explained in the remaining part of this section.

Figure 6 Overall structure of EcoDYN (see online version for colours)

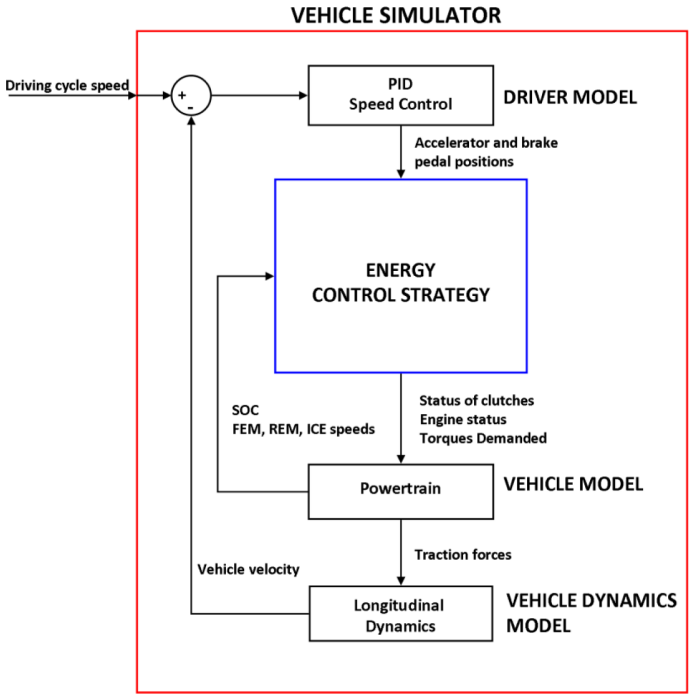

4.1 Driver model

The hybrid vehicle modelled has a single speed gearbox and the engagement of the two clutches is commanded by the supervisory control. Therefore the only driver inputs modelled in EcoDYN are accelerator and brake pedal positions and the steering wheel input. On a straight line motion where the steering wheel input is zero such as the case for the driving cycle simulations, the driver model for accelerator and brake pedal positions are computed by a PID controller representing the driver, expressed as:

$$\alpha / \beta = k_p \left(V_{\text{cyc}} - V\right) + k_i \int \left(V_{\text{cyc}} - V\right) \mathrm{d}t + k_d \frac{\mathrm{d}}{\mathrm{d}t}\left(V_{\text{cyc}} - V\right) \tag{12}$$

where α and β represent the accelerator and brake pedal positions depending on the sign of the PID output, and V_{cyc} is the driving cycle speed.

4.2 Powertrain model

The emphasis is given to the brake system and hybrid powertrain modelling in this section since the braking control strategy proposed in this study considers blending regenerative motor braking with wheel friction braking. For the rest of the powertrain such as the engine, differentials and halfshafts, the reader is referred to Biasini (2010).

4.2.1 EHB model

The isolated brake circuit is composed of a pump, high pressure reservoir, inlet or outlet valve and wheel brake cylinder for each wheel, and a low pressure reservoir. The isolated brake circuit and the dynamic variables for the portion of the circuit for a single wheel are shown in Figure 7(a) and (b) respectively.

The pump works in order to maintain a specific pressure in the reservoir. The delivered flow rate is calculated from a look-up table with the pressure difference as the input, as illustrated in Figure 8 (Borchsenius, 2003).

$$q_p = f(p_{acc} - p_a). \tag{13}$$

Figure 7 An illustration of the hydraulic circuit: (a) the electro-hydraulic brake circuit (1) pump (2) high pressure reservoir, (3) inlet valve, (4) outlet involved in the model valve, (5) wheel brake cylinder, (6) reservoir at ambient pressure and (b) illustration of the dynamic variables (see online version for colours)

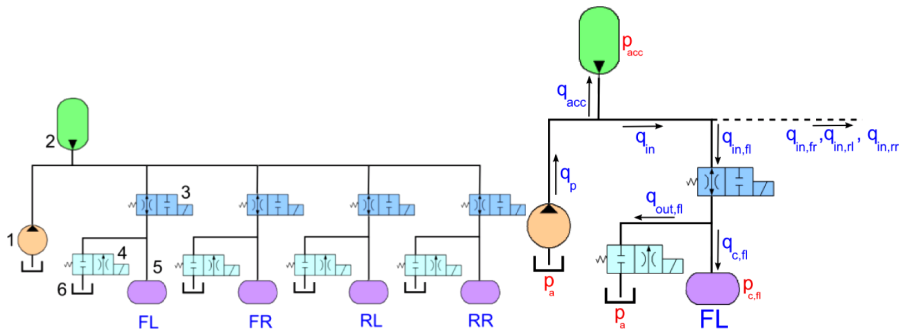

Figure 8 The pump characteristic for the flow rate vs. the input-output pressure difference (see online version for colours)

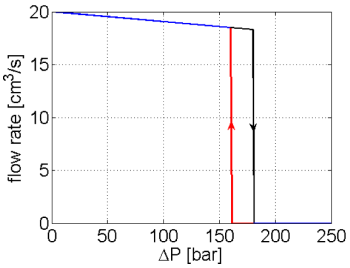

The reservoir is simulated as a hydro-pneumatic accumulator, which contains a bubble with gas that has greater compressibility than the hydraulic fluid. The accumulator is

therefore able to absorb and deliver a relatively high quantity of hydraulic fluid. Based on the Poisson equation, the non-linear differential equation for the accumulator pressure can be written as (Backe et al., 1994)

$$\dot{p}_{acc} = \frac{q_{acc}\kappa p_{acc}}{V_o}\left(\frac{p_{acc}}{p_o}\right)^{1/\kappa} \tag{14}$$

where κ is the polytropic gas index and V_o is the initial volume of the fluid in the accumulator.

The valves are modelled as an orifice with a continuously controllable cross-section. The Bernoulli equation to calculate the valve flow can be written as (Beater, 1999)

$$q_{I/Oi} = Au_{I/Oi}\alpha\sqrt{\frac{2}{\rho}(p_{in} - p_{out})} \tag{15}$$

where $q_{I/Oi}$ is the fuel flow rate across the ith inlet or outlet valve, A is the orifice cross-section, α is the flow coefficient, ρ is the fluid density, and $u_{I/Oi}$ is the controlled input for pressure modulation. The flow rate vs. the pressure difference is shown in Figure 9(a).

The wheel brake cylinder consists of a cylinder with a piston. The hydraulic fluid flows into the cylinder and pushes the piston with the friction pads onto the brake disc. The system is based on a lookup table that calculates the cylinder pressure from the cylinder volume, as given in Figure 9(b) (Seewald, 1997).

$$V_c = \int q_c \mathrm{d}t \tag{16}$$

$$p_c = g(V_c) \tag{17}$$

The last component of the brake system is the brake discs. The brake torque is calculated simply as:

$$T_b = 2\mu_B r_B A_B (p_c - p_a) \tag{18}$$

where μ_B is the brake disc friction coefficient, r_B is the radius between the contact point and centre of the wheel, and A_B is the brake disc friction area.

Figure 9 Valve and wheel brake pressure characteristics: (a) the inlet valve characteristics at wide open and (b) the wheel brake pressure as a function of the condition fluid volume in the cylinder (see online version for colours)

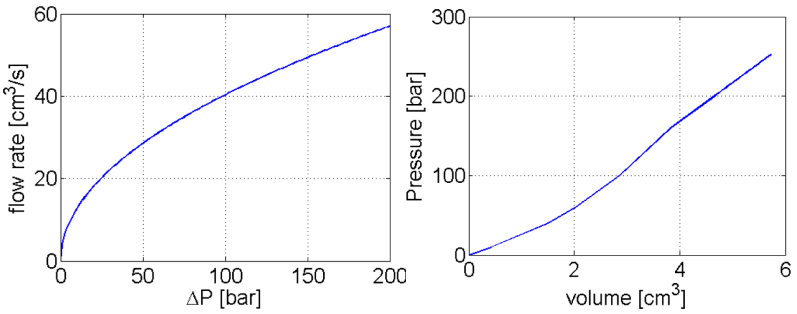

(a) (b)

4.2.2 Hybrid powertrain model

In this subsection, the defining equations for the battery and the motor models are given. The battery of the OSU EcoCAR vehicle is a 21 kWh lithium ion battery pack, composed of three modules in parallel, with each module consisting of 110 cells in series, as shown in Figure 10(a).

The battery model used in EcoDYN is a zero-th order battery model used to estimate the battery SOC. The equivalent circuit that represents the battery is shown in Figure 10(b). The voltage at the battery terminals V_{batt} is given by

$$V_{batt} = V_{oc} + R_{batt} I_{batt} \tag{19}$$

Figure 10 Battery modelling: (a) battery architecture of the OSU EcoCAR and (b) equivalent circuit representing the battery vehicle (see online version for colours)

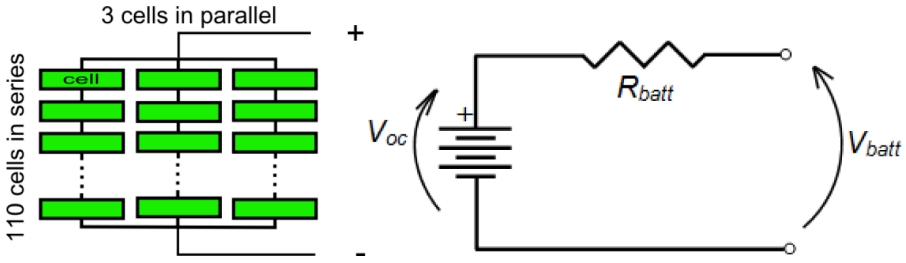

(a) (b)

where I_{batt} is the battery current, R_{batt} and V_{oc} are the equivalent battery resistance and open circuit voltage which can be represented as functions of SOC of the battery respectively. Measured data for the open circuit voltage as a function of the state of charge for a single cell is shown in Figure 11.

Battery power can be obtained by multiplying both sides of equation (19) by battery current I_{batt}, and battery current can then be derived in terms of the battery power, open circuit voltage and the equivalent resistance as:

$$I_{batt} = \frac{\sqrt{V_{oc}^2 - 4R_{batt}P_{batt}} - V_{oc}}{2R_{batt}}. \tag{20}$$

Using equation (20), battery efficiency during charging can be derived as

$$\eta_{batt} = \frac{V_{oc}I_{batt}}{P_{batt}} = \frac{V_{oc}\sqrt{V_{oc}^2 - 4R_{batt}P_{batt}} - V_{oc}^2}{2R_{batt}P_{batt}}. \tag{21}$$

Note that the battery efficiency is the reciprocal of the expression given in equation (21) during discharging as it is defined as $P_{batt}/V_{oc}I_{batt}$ for discharging.

The battery power on the other hand is composed of the motor power requests and the auxiliary load that can be expressed by:

$$P_{batt} = P_{acc} + \sum_i T_i\omega_i \begin{Bmatrix} \dfrac{1}{\eta_i(\omega_i, T_i)} & T_i \geq 0 \\ \eta_i(\omega_i, T_i) & T_i < 0 \end{Bmatrix} \tag{22}$$

where P_{acc} is the electrical load of the accessories assumed to be constant, T_i and ω_i are the motor speed and torque and η_i is the combined energy conversion efficiency of the ith electric machine (FEM or REM) and its power converter. The efficiency map for the front electric motor is shown in Figure 12.

Figure 11 Open circuit voltage as a function of state of charge (see online version for colours)

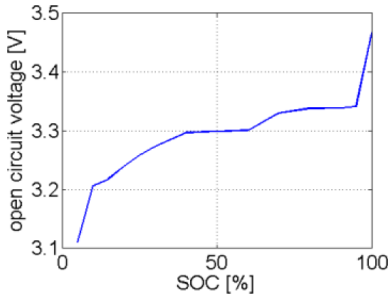

Figure 12 The efficiency contours as a function of speed and torque for the front electric motor (see online version for colours)

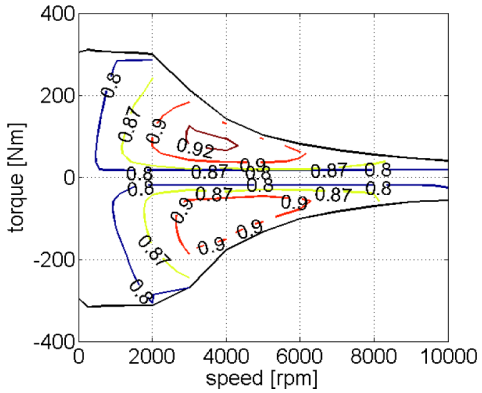

The motor, differential, half shafts and the wheels are illustrated in Figure 13. The electrical response characteristics of the permanent magnet electric motors are represented by a first order system since the electric machines exhibit a short time lag between the torque request and the actual torque (Kim et al., 2008). The equation representing this relation can be expressed by:

$$\tau \frac{\mathrm{d}T_{act}}{\mathrm{d}t} + T_{act} = T_{req} \tag{23}$$

and the equation of motion for electric motor speed:

$$J_{em}\dot{\omega}_{em} = T_{act} - T_{diff} \tag{24}$$

where T_{req} and T_{act} are the requested and realised torque respectively, J_{em} is the motor output shaft rotational inertia and T_{diff} is the resistive torque at the input of the differential.

Figure 13 An illustration of the motor, differential, half shafts and wheels

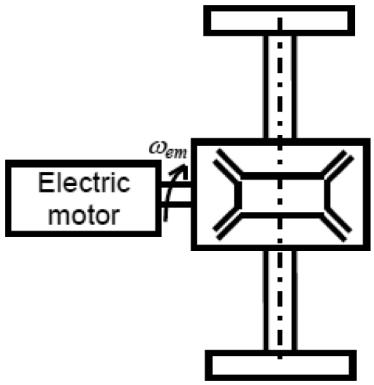

4.2.3 Vehicle dynamics model

EcoDYN assumes four degrees of freedom vehicle dynamics model, namely longitudinal and lateral motion, and yaw and roll motions. However, considering the drive cycle simulations performed in the next section where the motion is a straight line motion, the equation of motion in longitudinal direction is sufficient for representing the vehicle dynamics.

$$M\frac{\mathrm{d}V}{\mathrm{d}t}\sum_{i=1}^{4}F_{xi}-F_a-F_r \tag{25}$$

where F_a and F_r are air and rolling resistance expressed by equations (2) and (3) respectively, F_{xi} is the longitudinal force generated by the ith tyre, represented by the Pacejka formula (Pacejka, 2003) as:

$$F_{xi}=\mu F_{zi}\sin(C_{xi}\arctan(B_{xi}s_i-E_{xi}(B_{xi}s_i-\arctan(B_{xi}s_i)))) \tag{26}$$

where μ is the coefficient of adhesion, B_{xi}, C_{xi} and E_{xi} are tyre parameters, s_i is the longitudinal slip for the ith wheel and F_{zi} is the dynamic normal load on the ith wheel represented as:

$$\begin{aligned}
F_{zfl}&=\frac{Mgb}{2l}-\frac{Ma_xh}{2l}\\
F_{zfr}&=\frac{Mgb}{2l}-\frac{Ma_xh}{2l}\\
F_{zrl}&=\frac{Mga}{2l}+\frac{Ma_xh}{2l}\\
F_{zrr}&=\frac{Mga}{2l}+\frac{Ma_xh}{2l}
\end{aligned} \tag{27}$$

where M is the total mass of the vehicle, a and b are distances form front and rear axles to the centre of mass, and l is the wheelbase.

4.2.4 Control strategy

The Energy Control Strategy, as implemented in EcoDYN simulator, is composed of two layers, as shown in Figure 14: the Supervisory Control Strategy and the Energy Management Strategy.

The Supervisory Control Strategy decides the state of the clutches, i.e., the driving mode, depending on SOC, vehicle speed and pedal positions. OSU EcoCAR vehicle's twin-clutch transmission allows the vehicle to operate in multiple modes, to optimise vehicle performance under various driving conditions. Different operating modes depending on the status of the clutches are shown in Figure 15.

Figure 14 An illustration of the control strategy (see online version for colours)

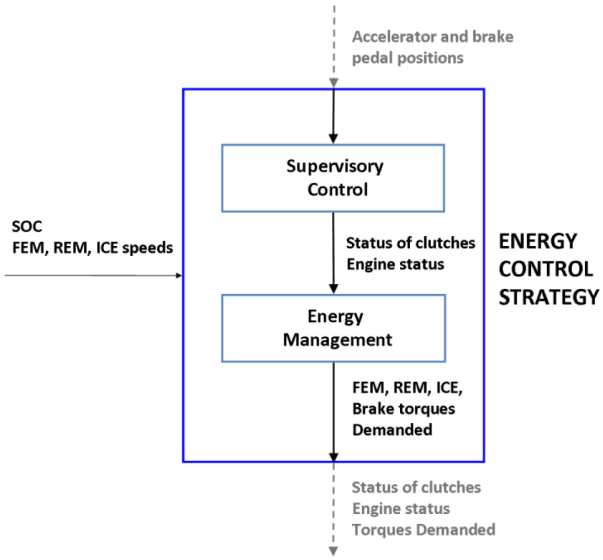

Figure 15 An illustration of the different operating modes of operation (see online version for colours)

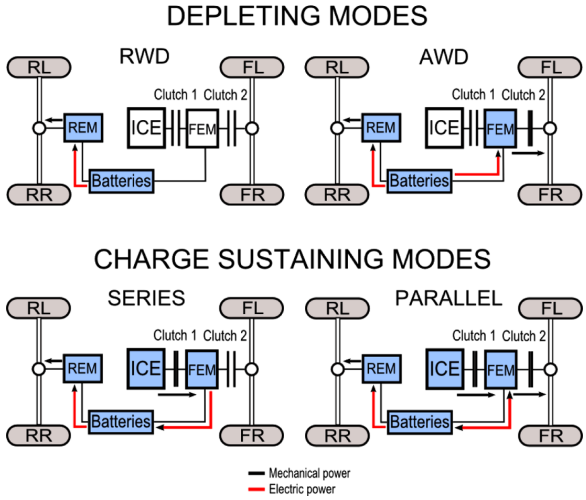

During braking, i.e., when the brake pedal is depressed, the Supervisory Control Strategy commands the disengagement of Clutch 1 and the engagement of Clutch 2 (top right mode in Figure 15). In this operating mode both electric motors are connected to the wheels so that both axles can be utilised for regenerative braking while the ICE is disconnected from the powertrain in order to avoid the energy dissipation caused by engine drag. The presence of an electric motor on each axle and the EHB system allows achieving the optimal brake torque distribution on both axles using motor braking exclusively in most of the braking manoeuvres. The two-way split proposed is as follows:

Total braking force: Total braking force F_B is decided by the driver who acts on the brake pedal where the brake force is a non-linear function of the brake pedal position as shown in Figure 16(a) until the ABS control is activated. Drivers prefer to have a low level of braking force sensitivity during the first part of the pedal stroke and a fast increment of the braking force in the last part of the pedal stroke (abrupt braking).

In addition to the force as a function of the brake pedal position, emulated engine drag is also taken into account. Considering the engine drag torque as a function of engine speed, the emulated engine drag force as a function of vehicle speed can be generated as shown in Figure 16(b).

Figure 16 Components specifying the brake force request: (a) brake force as a function of pedal position and (b) emulated engine drag (see online version for colours)

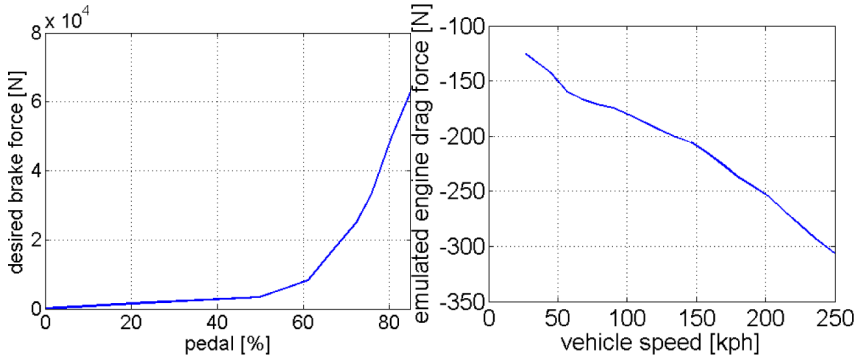

(a) (b)

So the brake force request can be expressed as:

$$F_b = f(\beta) + F_{be}(V) \tag{28}$$

Front-rear braking force split: An ideal brake force distribution factor can be defined by which both front and rear wheels lock simultaneously. An expression for such an ideal distribution factor as a function of the total braking force can be derived as (Biasini, 2010):

$$\begin{aligned} F_{bf} &= \left(\frac{b}{l} + \frac{h}{l}\frac{F_b}{\mathrm{Mg}}\right) F_b \\ F_{bf} &= \left(\frac{a}{l} - \frac{h}{l}\frac{F_b}{\mathrm{Mg}}\right) F_b \end{aligned} \tag{29}$$

where b is the distance between centre of gravity of the vehicle and rear axle, l is the wheelbase, and h is the height of centre of gravity. The ideal distribution is shown in Figure 17.

Figure 17 Graphical method for obtaining the brake force distribution when the total braking force is assigned (see online version for colours)

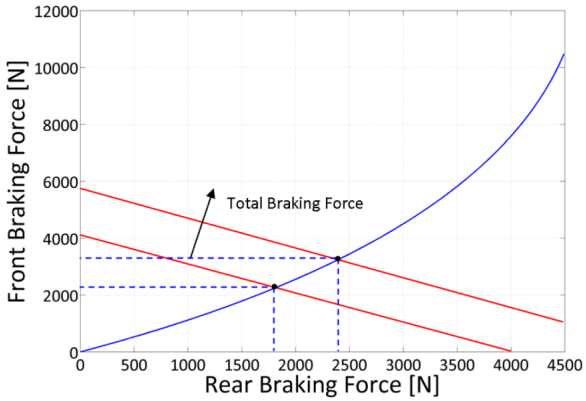

In conventional vehicles equipped with a standard hydraulic brake system directly actuated by the master cylinder, it is not possible to change the braking distribution factor continuously in real time. The problem is partially solved by the adoption of appropriate devices such as a proportioning valve which allows approximation of the parabolic ideal brake force distribution factor with a polygon curve with 1 or 2 angles (Bosch, 2005). On the other hand, BBW type systems which use the existing ABS system's hydraulics and sensors with the addition of improved valves are getting more popular especially among EVs and HEVs of the last generation, and the aim of reaching an ideal braking force distribution factor can be achieved in most of the driving conditions.

Note that the analysis above considers the knowledge of mass as a priori. This can be realised with a measurement unit such as the one proposed in Spelta et al. (2010).

Motor-friction brake force split: once the braking force for each axle is set, the distribution of the braking force between the electric motors and the friction braking needs to be defined in order to obtain the maximum value of the regenerated power into the battery at each instant:

$$P_{net} = -\eta_b \left(P_{aux} + \sum_i T_i \omega_i . \eta_i(\omega_i, T_i) \right) \tag{30}$$

where P_{aux} is the auxiliary power assumed to be constant and η_b is the battery efficiency expressed by equation (21). Since the auxiliary load does not depend on the power regenerated by the motors, it is sufficient to maximise (magnitude wise) the second term on the right hand side of equation (30). The control of each electric motor can be handled independently to reach the optimal solution. Considering the optimisation of each electric motor instead of the optimisation of their sum can cause a potential problem if the battery power limitation is taken into consideration as a constraint. However, the lithium-ion battery pack used in EcoCAR vehicle has a maximum limit of 300 Amps of current during charging which is higher than the sum of the currents that the two motors can

provide. This can be verified by substituting the sum of the power ratings of the two motors into equation (20). This is also verified by simulation results in the next section.

So the optimisation problem can be formulated as:

$$T_i^* = \arg\max\left(|\, T_i \omega_i \eta_i(\omega_i, T_i)\,|\right) \tag{31}$$

with the constraints being

$$\begin{aligned} &0 \le |T_i k_i \eta_{ti}| \le |T_{bi}| \\ &|T_i| \le |T_i(\omega_i)|_{max} \\ &\omega_{i\,min} < \omega_i \\ &\mathrm{SOC} < \mathrm{SOC}_{max} \end{aligned} \tag{32}$$

where T_i^* is the motor torque value for the ith motor (front or rear) that maximises the net power stored in the battery, k_i and η_{ti} are the transmission ratio and efficiency of the ith electric motor, T_{bi} is the torque for the ith axle specified by the first level of split, namely using equation (29), $|T_i(\omega_i)|_{max}$ is the maximum (magnitude wise) electric motor torque depending on motor speed (refer to Figure 12), ω_{imin} is the motor threshold speed for regenerative braking, and SOC_{max} is the maximum SOC of the battery for which regenerative braking is allowed.

Once the electric motor torque is specified, the friction brake torque command is obtained by substituting the motor torque command from the total torque desired as:

$$T_{fbi} = T_{bi} - T_i k_i \eta_{ti} \tag{33}$$

EHB pressure control adopted: The control adopted is a closed loop control on the brake caliper pressures. The inputs and outputs are the desired braking torques T_{fbi} as explained in the previous sections and the actual braking torques T_{bi} at each wheel respectively, as illustrated in Figure 18.

Figure 18 Block scheme of the EHB pressure control

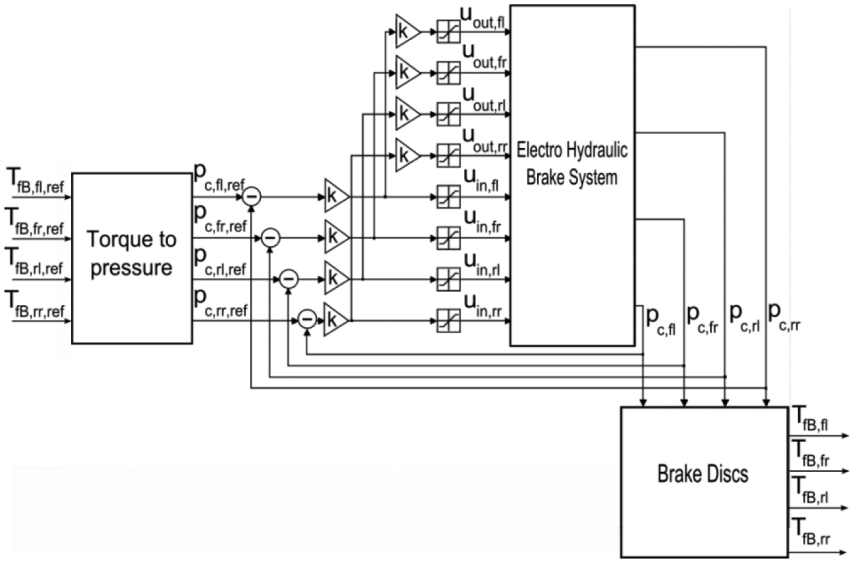

The first block on the left is used to convert the desired torque to desired pressure values. The difference between the desired pressure and the pressure measured for each calipers is amplified by the gain k which has a marginal importance, since it is preferable not to operate in a condition where the valve is partially open in order to avoid a slow system response. Saturation with a range of 0–1 is used after the gains because of limits of the cross sectional areas of the valves (refer to equation (15)). For the outlet valve there is an ulterior gain of –1 before the saturation. Therefore if the objective is to increase the pressure in the caliper the corresponding inlet valve is opened and the outlet valve is closed, and vice versa if the target is to decrease the pressure in the caliper.

The response of the EHB system is depicted in Figure 19 when the input is a step of 180 bar followed by a complete pressure release. The time response characteristics of the system shows that 80 bar of effective pressure is reached inside the calipers in approximately 50 milliseconds. This value is well below the limit of 120 ms as imposed in Reuter et al. (2003).

Figure 19 EHB response for a step of 180 bars of desired pressure (see online version for colours)

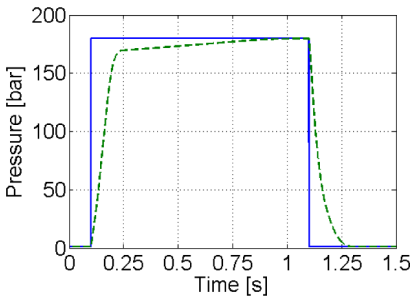

5 Simulation results

Two simulation scenarios are considered: the constant brake pedal, and driving cycles simulations.

5.1 Constant pedal travel

The first scenario is braking with a constant brake pedal travel which characterises a driver with a desire of constant deceleration rate. For this case the driver model is kept out of the loop and a step input for the brake pedal position is commanded at 38 s when the vehicle speed is 108 kph. The results for a pedal position of 50, 60 and 65% are depicted in Figures 20–22 respectively. The figures are structured such that front and rear EHB friction torque and motor torque values are shown at the 1st row 1st column, vehicle speed is shown in the 1st row 2nd column, desired and actual brake force values for front and rear axles are shown in the 2nd row 2nd column, the brake pedal percentage and deceleration in units of g is given in the 2nd row 2nd column, SOC of the battery is given in 3rd row 1st column and battery power and current are given in 3rd row 2nd column.

During these braking manoeuvres, the requirements that should be satisfied by the proposed braking strategy are:

- The desired force for front and rear wheels as specified by equations (28) and (29) should be satisfied. The plot showing the desired and actual force (2nd row 1st column) values for front and rear axles show that this condition is satisfied as the actual force values reach within 90% of the desired values within less than a second.
- Smooth deceleration should be satisfied since the brake pedal travel is constant. The plot showing the deceleration and pedal (2nd row 2nd column) shows that the deceleration is smooth for all three cases. In Figure 20 where the pedal is 50%, although the braking force is dominant, the effect of aerodynamic resistance can also be observed. As the vehicle slows down, the aerodynamic resistance decreases as specified by equation (2), causing a slight decrease in deceleration. This effect is not quite clear in Figures 21 and 22 as the highly dominant decelerating force is the brake force for these cases.
- Smooth transition from motor braking torque to EHB friction torque should be satisfied. The motor braking torque is disabled below a specific motor threshold speed as dictated by the proposed control strategy. As the motor reaches this speed, motor regenerative braking torque drops to zero and EHB friction torque supplies the demanded braking torque. This can be seen at the 55th second in the top left plot of Figure 20, as the front electric motor threshold speed is reached corresponding to a vehicle speed of 8 kph and the front EHB friction torque starts supplying the demanded braking torque. The same behaviour can be observed also for the rear powertrain as around the 56th second for the rear electric motor corresponding to a vehicle speed of 4 kph (the gear ratio for the rear electric motor is almost twice the gear ratio of the front one) the motor torque is cut and braking is provided by EHB friction braking.

  During this transition, due to different internal dynamic characteristics of the EHB system and electric motors, there is a slight deviation of actual force for the front axle from the desired one, as can be seen in the force plots (2nd row 1st column). This is due to the fact that the EHB system realises the torque compensation as commanded by the control with a delay. This can be avoided by appropriate filtering of the control signals before feeding them into the actuators, namely the motors and the EHB system. Although, that slight deviation of force does not cause a major roughness with the deceleration as can be seen in the plot showing deceleration values for three different braking manoeuvres.
- The battery current and power should not approach the physical limits of the battery for battery durability issues. As seen in the plot showing the battery current (3rd row 2nd column) the current is well below the limit of 300 amps for charging.

As a final observation for these simulation results, it is seen that the rise in the SOC of the battery is 1, 0.6 and 0.45% in Figures 20–22 respectively. This is an expected result as the motors are providing regenerative braking torque for a longer duration of time for lower decelerations.

To analyse the energy efficiency, similar simulations are performed with different initial speeds (1–40 m/s) and deceleration (1–9 m/s^2) values. The results are collected in Figure 23.

Figure 20 Vehicle response for a constant brake pedal travel of 50% (see online version for colours)

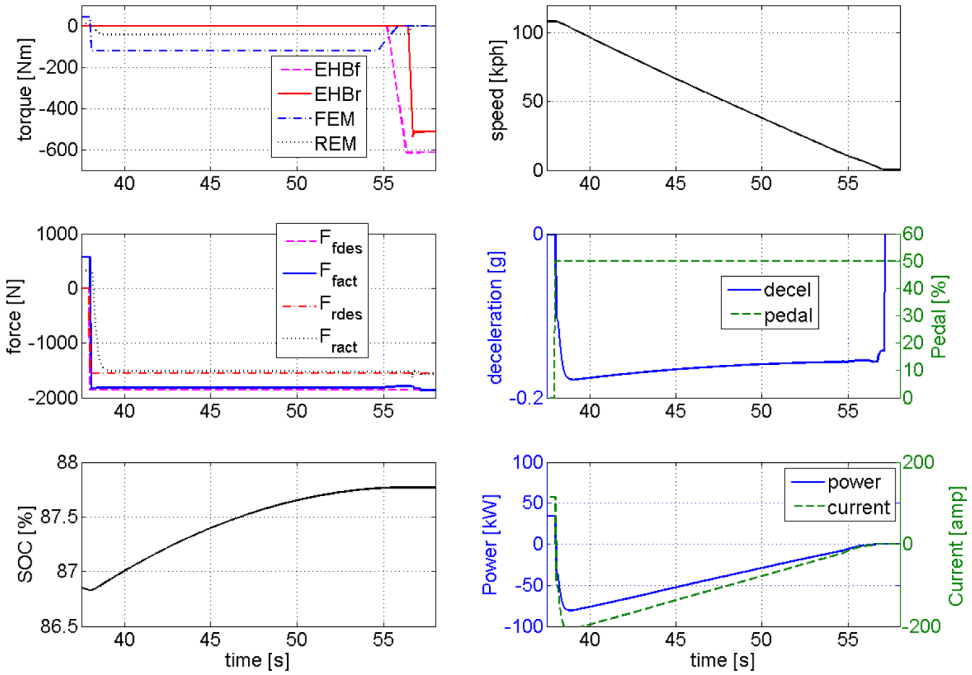

Figure 21 Vehicle response for a constant brake pedal travel of 60% (see online version for colours)

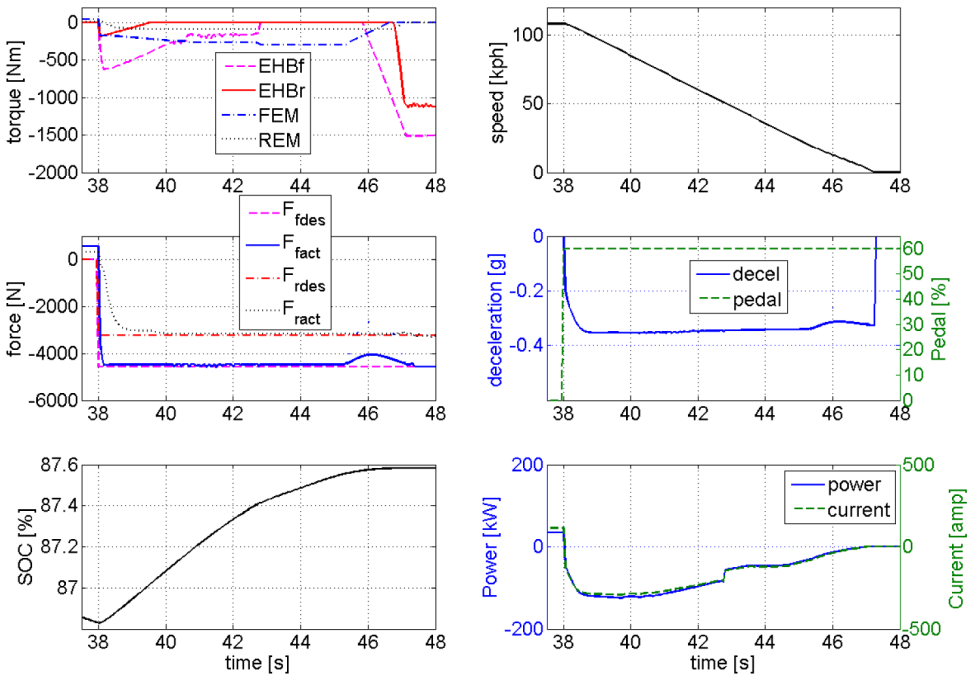

Figure 22 Vehicle response for a constant brake pedal travel of 65% (see online version for colours)

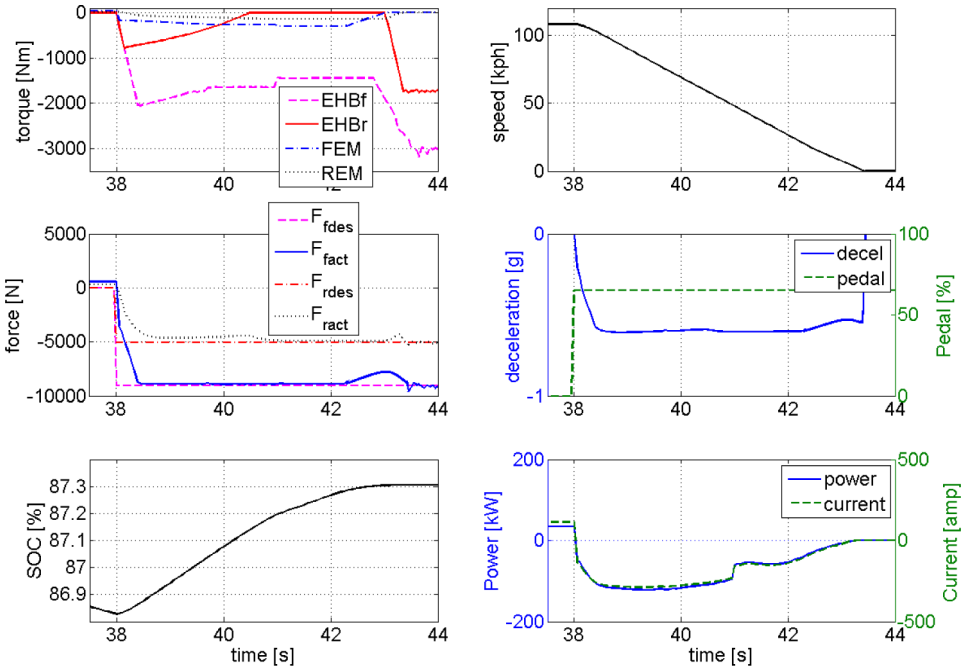

Figure 23 The percentage of vehicle kinetic energy that is recovered in the battery, for braking manoeuvres with different initial speed and deceleration rates (see online version for colours)

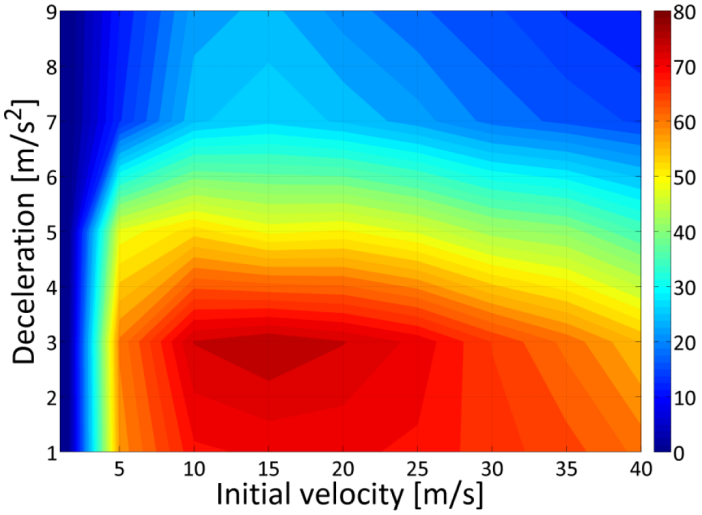

It is observed from the figure that for high initial speeds and decelerations the recuperated energy efficiency is low, in fact, the electric motors work in saturation and a certain amount of vehicle kinetic energy is simply converted to heat by friction brakes. Results are similar for low initial speeds since the motors work at low speed region where

the regenerative braking is not very efficient; also in this case EHB friction brake system is utilised more. For low-medium value of deceleration (lower than 4 m/s^2) and for medium-high initial vehicle velocity (higher than 10 m/s) simulation results show a higher efficiency. In this situation both the battery and the electric motors work in their high efficient region.

5.2 Drive cycle simulations

Simulations to assess the efficiency of the proposed braking strategy are performed for the FUDS, FHDS and US06 drive cycles as depicted in Figure 24. The proposed strategy is compared with a parallel braking strategy which distributes 60 and 40% of the total braking force to the front and rear axles, respectively, and commands motor braking corresponding to an amount of 30% of the friction braking (if it is available and convenient) on each axle. The choice of these values is suggested by the automotive industry. This strategy corresponds to a reasonable parallel braking strategy that could be applied to a hybridised stock vehicle such as the EcoCAR vehicle for which there is no control authority on friction brakes. The proposed control strategy is also compared with pure friction braking strategy, i.e., having to regenerative motor braking. Pure friction braking strategy is taken as a reference point to evaluate the enhancement on net energy consumption for the other two strategies.

Figure 24 FUDS, FHDS and US06 driving cycles, from top to bottom respectively (see online version for colours)

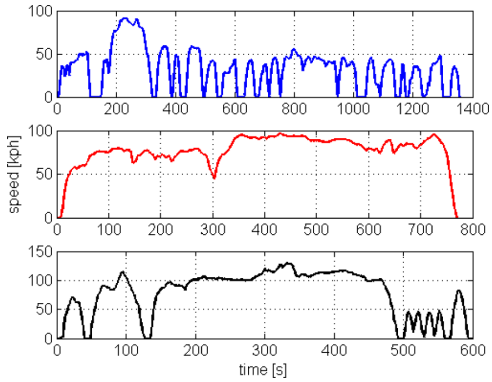

The tabulated results show the brake energy E_b in the first row, computed by the expression:

$$E_B = \sum_{i=1}^{4} \int_{cyc} \omega_i T_{bi} \mathrm{d}t \tag{34}$$

where ω_i is the rotational speed of the ith wheel and T_{bi} is the net braking torque for the ith wheel. Note that this is the total braking energy computed differently by approximations in Section 2 with the expression given in equation (11).

On the second row of Table 3 the net energy stored in the battery E_{net} is given. This is computed by:

$$E_{net} = \int_{I_{batt}<0} VOC.I_{batt}\,dt \tag{35}$$

On the third row the regenerative braking energy efficiency is given which is computed by E_{net}/E_B*100. On the fourth and fifth rows of the table, the drop in SOC of the battery ΔSOC during pure electric operation of the vehicle (when the initial SOC is taken as 90%), and fuel consumption FC during charge sustaining operation of the vehicle (when the initial SOC is taken as 30%) are given respectively. These values show the impact of the braking strategy on energy consumption of the vehicle, during both modes of operation. On the fifth row, the fuel economy improvement in comparison to the no-regen scenario is given during charge sustaining operation of the vehicle.

Table 3 Drive cycle simulation results

	Proposed	*Parallel*	*No regen*	*Proposed*	*Parallel*	*No regen*	*Proposed*	*Parallel*	*No regen*
	FUDS			*FHDS*			*US06*		
E_B [MJ]		3.17			0.71			3.22	
E_{net} [MJ]	2.51	0.44	–	0.31	0.12	–	1.87	0.55	–
η_{regen}	79.2	13.9	–	43.6	16.9	–	58.1	17.1	–
ΔSOC [%]	14.1	16.9	17.6	23.1	23.8	24.0	25.0	28.3	30.0
Gain [%]	20	4	–	3.8	1	–	17	6	–
FC [l/100 km]	6.27	7.61	7.95	7.34	7.57	7.62	7.82	8.47	8.82
Gain [%]	21	4	–	4	1	–	11	4	–
FE improvement [mpg]	7.93	1.33	–	1.18	0.21	–	3.42	1.11	–

The first observation is that the brake energy E_B for each cycle given in Table 3 obtained by the simulations is slightly higher than the values found in Section 2 by the preliminary energy analysis, namely in the 1st paragraph of Page 8. One of the reasons of this difference is that the preliminary energy analysis neglects the powertrain efficiencies between the motors and the wheels that have a crucial role in specifying the braking energy. Another reason for this difference is that the assumption of knowing the drive cycle as a priori for the preliminary energy analysis yields zero braking for decelerations that can be caused only by rolling and aerodynamic resistances. On the other hand the PID driver model in the simulator applies braking to fit the drive cycle even when resistances are sufficient to decelerate the vehicle at a low rate. Therefore, the simulator applies the brakes more which contribute to this difference in brake energy for the two approaches.

The second observation is the regenerative braking energy efficiencies. For FUDS, the efficiency is quite higher that the efficiencies for the other cycles. This is an expected result since in this cycle the required braking torque can be supplied by the electric motors exclusively with a high efficiency for most of the deceleration events. For the US06 cycle, although the braking energy E_B is greater than the one for the FUDS cycle, due to a sharper deceleration trend in this cycle the motor braking is not sufficient

occasionally and the EHB friction brakes are applied. This causes a regen efficiency of 58.1%. For the FHDS cycle on the other hand, there are just a few sharp decelerations which yield low values for both E_B and E_{net}.

The last observation is the reflection of the regen efficiencies on ΔSOC and FC during electric and charge sustaining modes of operation the vehicle respectively. The percent gain (with respect to the results for the no regen strategy) for ΔSOC and FC reaches 20% and 21% respectively, for FUDS, and 17% and 11% respectively, for US06 whereas for the parallel regen braking strategy this improvement is 4% and 4% for ΔSOC and FC respectively, for FUDS, and 6% and 4% for ΔSOC and FC respectively, for US06. These results show the superiority of the proposed control strategy to the parallel strategy in terms of regen efficiency and energy recuperation, which is an expected result.

6 Conclusions

In this work regenerative braking for an E-REV has been investigated in terms of both brake system modelling and proposing a control strategy. In particular an EHB system is modelled and implemented to the OSU Eco-CAR simulator.

The proposed regenerative braking strategy achieves the dual objective of ensuring a good dynamic performance of the vehicle by applying the ideal brake force distribution and maximising the energy recovered by drawing advantage of the axle motors which allows the regenerative braking on both axles.

Although the proposed control considers a vehicle architecture with two axle motors, the two-layered split structure of the braking strategy can be easily modified for implementation to different vehicle architectures. For instance, in the very common case of an HEV with a single axle motor, it would be possible to modify the distribution of the braking torque by increasing the amount of motor braking on one axle and compensating this with EHB friction braking on the other axle for stability purposes. Consequently, the second split between the electric and friction torque could be applied only to the motorised axle.

Simulation results can be analysed to figure out some important considerations: the effectiveness of regenerative braking depends mainly on the driving condition. It is shown by simulations that the E-REV equipped with the EHB system and axle motors together with the proposed control strategy can go up to 80% regen efficiency that would yield saving 21% of fuel in urban driving condition. These results can lead to the adoption of this vehicle layout and control strategy, for instance, in the case of EVs and PHEVs. The initial cost due to the implementation of the EHB system can be recovered during the vehicle life time thanks to the enhanced energy economy. Moreover, it is disputable that the adoption of two electric motors (one per axle) conducts to an increment of the cost and/or weight of the vehicle, although this solution is more cumbersome and increases the vehicle layout complexity. It is shown in Hellgren et al. (2007) that having a big electric motor which provides all the vehicle electric power in comparison to the case of having two smaller motors, each supplying one half of the total vehicle electric power, is actually worse in terms of weight and cost.

References

Ahn, J.K., Jung, K.H., Kim, D.H., Jin, H.B., Kim, H.S. and Hwang, S.H. (2009) 'Analysis of a regenerative braking system for hybrid electric vehicles using an electro-mechanical brake', *International Journal of Automotive Technology*, Vol. 10, No. 2, pp.229−234.

Backe, W. and Murenhoff, H. (1994) *Grundlagen der olhydraulik, umdruck zur vorlesung*, Institut fur fluidtechnische Antriebe und Steuerungen der Rheinisch-Westfalischen Hochschule Aachen, Auflage. p.10.

Bayar, K., Bezaire, B., Cooley, B., Kruckenberg, J., Schacht, E., Midlam-Mohler, S. and Rizzoni, G. (2010) 'Design of an extended-range electric vehicle for the EcoCAR challenge', *Proceedings of the ASME International Design Engineering Technical Conferences & Computers and Information in Engineering Conference*, Montreal, Quebec, Canada, pp.687–700.

Beater, P. (1999) *Entwurf Hydraulischer Maschinen*, Springer, Berlin.

Biasini, R. (2010) *Modeling and Control of the Regenerative Brakin System for a Hybrid Electric Vehicle with Axle Motors*, Master of Science Thesis, Universita di Pisa.

Borchsenius, F. (2003) 'Simulation olhydraulischer systeme', *Fortschritt-Berichte VDI*, Reihe 8 Nr. 1005, VDI-Verlag, Dusseldorf.

Bosch (2005) *Driving Stability Systems*, Robert Bosch GmbH Press, Plochingen, Germany.

Britto, J.F.F.H., Perondi, E. and Mazaffere, J.A.E. (2005) *Design of a Pneumatic Regenerative Braking System*, SAE Paper 2005-01-3969.

Clegg, S.J. (1996) *A Review of Regenerative Braking System*, University of Leeds Institute for Transport Studies, Working Paper 471.

D'alfio, N., Morgando, A. and Sorniotti, A. (2006) 'Electro-hydraulic brake systems: design and test through hardware-in-the-loop simulation', *Vehicle System Dynamics*, Vol. 44, pp.378–392.

Diego-Ayala, U., Martinez-Gonzales, P., McGlashen, N. and Pullen, K.R. (2008) 'The mechanical hybrid vehicle: an investigation of a flywheel-based vehicular regenerative energy capture system', *Proc. IMechE, Part D: J. Automobile Engineering*, Vol. 222, pp.2087–2101.

EcoCAR (2008) *EcoCAR Vehicle Competition Organized by Department of Energy and GM*, Available at http://www.ecocarchallenge.org

Gillespie, T.D. (1992) *Fundamentals of Vehicle Dynamics*, SAE publications, Warrendale, PA.

Hancock, M. and Assadian, F. (2006) 'Impact of regenerative braking on vehicle stability', *IEEE Hybrid Vehicle Conference*, IET The Institution of Engineering and Technology, pp.173–184.

Hellgren, J. and Jonasson, E. (2007) 'Maximisation of brake energy regeneration in a hybrid elecric parallel car', *Int. J. Electric and Hybrid Vehicles*, Vol. 1, No. 1, pp.95–121.

Hongyan, Z. and Tianjun, Z. (2009) 'Improving vehicle stability using electro-hydraulic braking system', *IEEE International Conference on Information Technology and Computer Science*, Kiev, Ukraine, Vol. 1, pp.593–596.

Jonner, W., Winner, H., Dreilich, L. and Schunck, E. (1996) *Electrohydraulic Brake System – The First Approach to Brake-by-Wire Technology*, SAE Technical Paper Series, pp.960–991.

Kepner, R.P. (2002) *Hydraulic Power Assist – A Demonstration of Hydraulic Hybrid Vehicle Regenerative Braking in a Road Vehicle Application*, SAE Paper 2002-01-3128.

Kim, D., Hwang, S. and Kim, H. (2008) 'Vehicle stability enhancement of four-wheel-drive hybrid electric vehicle using rear motor control', *IEEE Transactions on Vehicular Technology*, Vol. 57, No. 2, March, pp.727–735.

Lu, S., Corzine, K.A. and Ferdowsi, M. (2007) 'A new battery/ultracapacitor energy storage system design and its motor drive integration for hybrid electric vehicles', *IEEE Transactions on Vehicular Technology*, Vol. 56, No. 4, pp.1516–1523.

Mamilla, V.R. and Mallikarjun, M.V. (2009) 'Control of electro-mechanical brake with electronic control unit', *International Journal of Electronic Engineering Research*, Vol. 1, No. 3, pp.195–200.

Miller, J.M. (2004) *Propulsion System for Hybrid Vehicles*, The Institution of Electrical Engineers, London, UK.

Nakamura, E., Soga, M., Sakai, A., Otomo, A. and Kobayashi, T. (2002) *Development of Electronically Controlled Brake System for Hybrid Vehicle*, SAE Paper 2002-01-0300.

Pacejka, H.B. (2003) *Tire and Vehicle Dynamics*, Elsevier, Oxford, UK.

Reuter, D.F., Lloyd, E.W., Zehnder, J.W. and Elliott, J.A. (2003) *Hydraulic Design Considerations for EHB Systems*, SAE Paper 2003-01-0324.

Seewald, D. (1997) *Erstellung eines realitatsgetreuen, physikalischen erstatzmodells der mechanik und hydraulik eines anti-blockiersystems als basis fur ein mechatronisches gesamtmodell*, Diplomarbeit, MLaP, Paderborn.

Spelta, C., Delvecchio, D., Savaresi, S.M., Bonaccorso, G. and Ghirardo, F. (2010) 'Analysis of a sensor reduction in a semi-active suspension system for a 4-wheels vehicle', *3rd ASME Annual Dynamic Systems and Control Conference of*, Cambridge, MA, DSCC2010-4101, pp.1–6.

Tianjun, Z. and Changfu, Z. (2009) 'Research on electro-hydraulic brake system for vehicle stability', *IEEE International Conference on Industrial and Information Systems*, Haikou, China, pp.344–347.

Ueki, N., Kubo, J., Takayama, T., Kanari, I. and Uchiyama, M. (2004) *Vehicle Dynamics Electric Control Systems For Safe Driving*, Hitachi document. Available at http://www.hitachi.com/rev/field/electronics/__icsFiles/afieldfile/2004/11/26/r2004_04_104_3.pdf

Wang, F. and Zhuo, B. (2008) 'Regenerative braking strategy for hybrid electric vehicles based on regenerative torque optimization control', *Proceedings of the Institution of Mechanical Engineers, Part D: Journal of Automobile Engineering*, No. 4, pp.499–513.

Wang, F., Zhong, H., Mao, X., Yang, L. and Zhuo, B. (2007) 'Regenerative braking algorithm for a parallel hybrid electric vehicle with continuously variable transmission', *IEEE International Conference on in Vehicular Electronics and Safety*, *ICVES 2007*, Vols. 13–15, pp.1–4.

Xiang, W., Richardson, P.C., Zhao, C. and Mohammad, S. (2008) 'Automobile brake-by-wire control system design and analysis', *IEEE Transactions on Vehicular Technology*, Vol. 57, No. 1, pp.138–145.

Ye, M., Bai, Z. and Cao, B. (2008) 'Robust control for regenerative braking of battery electric vehicle', *IET Control Theory Appl.*, *2008*, Vol. 2, No. 12, pp.1105–1114

Yeo, H. and Kim, H. (2002) 'Hardware-in-the-loop simulation of regenerative braking for a hybrid electric vehicle', *Proceedings of the Institution of Mechanical Engineers, Part D: Journal of Automobile Engineering*, Vol. 216, pp.855–864.

Note

[1]Note that the segments of the drive cycles where resistances to motion are sufficient to decelerate the vehicle at the required rate, i.e., the deceleration segments where additional brake force is not required, are excluded in this energy analysis.

Abbreviations

HEV	Hybrid Electric Vehicle
EV	Electric Vehicle
PHEV	Plug-in Hybrid Electric Vehicle
E-REV	Extended–Range Electric Vehicle

Regen	Regenerative braking
EHB	Electro-Hydraulic Braking
EMB	Electro-Mechanical Braking
SUV	Sport Utility Vehicle
FEM	Front Electric Motor
REM	Rear Electric Motor
EcoDYN	EcoCAR vehicle simulator